Volume 4
Number 3
7 February 2023
Pages 717–978

Materials Advances

rsc.li/materials-advances

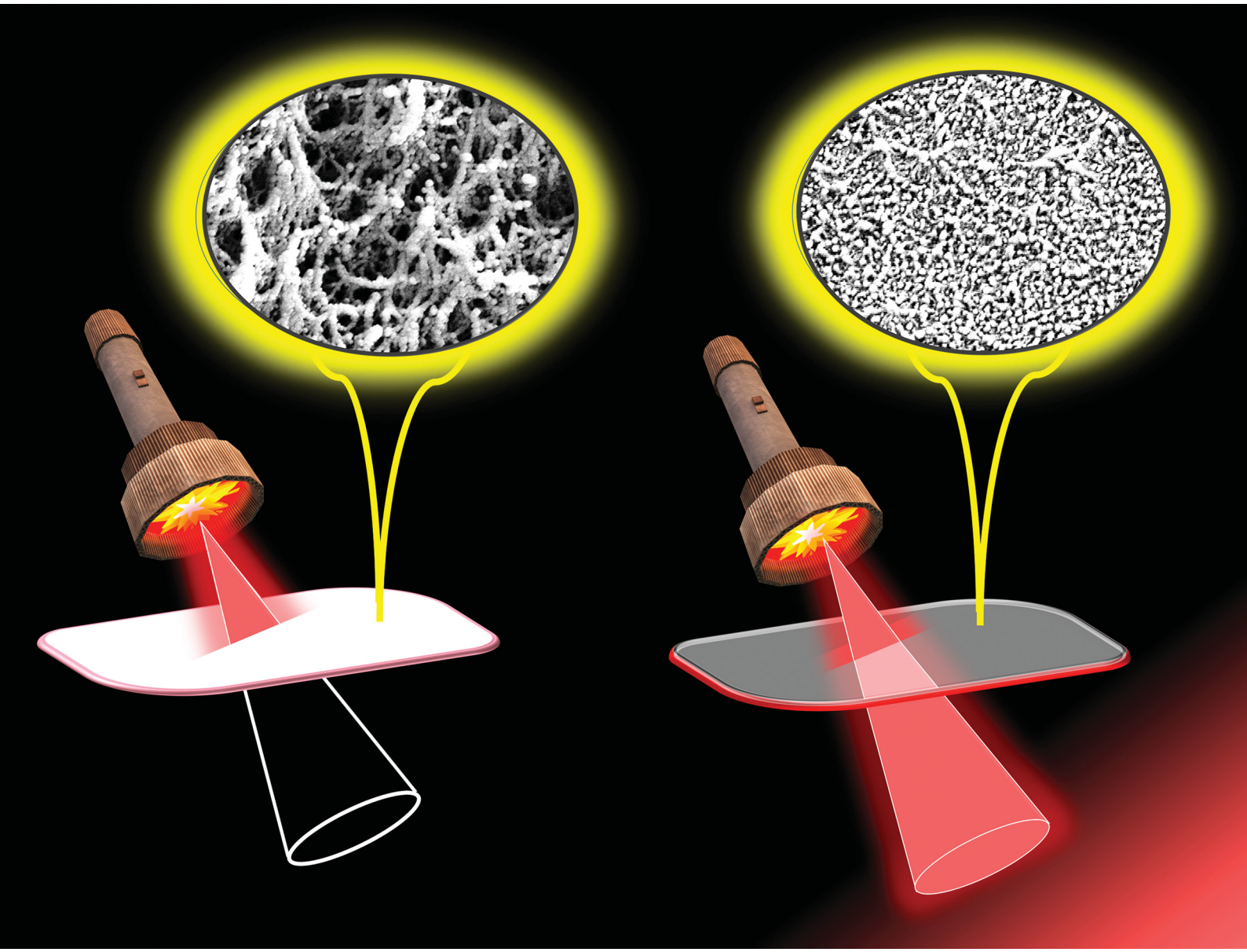

ISSN 2633-5409

ROYAL SOCIETY OF CHEMISTRY

PAPER
Baku Nagendra, Gaetano Guerra *et al.*
Transparent and flexible high-surface area nanoporous crystalline PPO films

Materials Advances

ROYAL SOCIETY OF CHEMISTRY

PAPER

View Article Online
View Journal | View Issue

Cite this: *Mater. Adv.*, 2023, 4, 881

Transparent and flexible high-surface area nanoporous crystalline PPO films

Baku Nagendra,* Syed Salman, Christophe Daniel, Paola Rizzo and Gaetano Guerra*

Received 13th October 2022,
Accepted 15th November 2022

DOI: 10.1039/d2ma00975g

rsc.li/materials-advances

Guest and processing conditions leading to high surface area (SA) nanoporous-crystalline (NC) poly(2,6-dimethyl-1,4-phenylene)oxide (PPO) films are explored. In this framework, we found crystallization conditions leading to unprecedented high-SA films (with SA up to 450 $m^2\ g^{-1}$) with transparency and toughness comparable with those for amorphous PPO films. Suitable preparation procedures require (i) guest-induced co-crystallization by large uptake of a highly boiling guest molecule; (ii) guest sorption from the vapor phase at a temperature close to the guest boiling point; and (iii) subsequent guest removal by sorption/desorption of a volatile guest. This high-SA, transparent, and tough NC PPO films are expected to be suitable for organic pollution remediation, molecular separations, and molecular sensing.

Introduction

Two thermoplastic and commercially available polymers, poly-(2,6-dimethyl-1,4-phenylene)oxide (PPO)[1–7] and syndiotactic polystyrene (sPS),[7–18] can be easily co-crystallized with low molecular-mass guest molecules. Moreover, PPO[19–26] and sPS[27–34] presently are the only two polymers, whose co-crystalline forms can lead to nanoporous-crystalline (NC) forms after suitable guest removal procedures.

The main feature of NC forms is their lower density than the corresponding amorphous phases, which leads to the high uptake of organic guest molecules, even when they are present only in traces. Uptake of guest molecules is particularly fast for PPO[35–37] and sPS[37–44] NC aerogels, due to their high surface area (SA; in the range of 500–750 $m^2\ g^{-1}$ and 200–350 $m^2\ g^{-1}$ for PPO and sPS, respectively). However, these very low-density aerogels present high per unit mass pollutant uptake, but relatively poor uptake per unit volume.

In recent papers,[45,46] we have shown that pollutant uptake per unit volume is much higher for low SA NC PPO films compared to for aerogels, provided that the crystalline phase chain axes, and hence, their intrahelical empty channels[23] are preferentially perpendicular to the film plane ($c_\perp$ orientation).[47,48] Moreover, for PPO and sPS NC polymer films with SA higher than 600 $m^2\ g^{-1}$ and 120 $m^2\ g^{-1}$, respectively, organic pollutant uptake is faster than for corresponding aerogels, even if evaluated per unit mass as was recently described.[49,50] Known preparation procedures for high-SA NC films require fast crystallization of the amorphous films, which is induced by high uptake (typically in the range 70–90 wt%) of non-volatile liquid guests (carvone or dibenzyl ether), followed by a guest exchange with a volatile guest. However, due to the presence of mesopores beside the nanopores of their crystalline phases, the described high-SA NC films are opaque and exhibit poor toughness, and hence, are unsuitable for many applications.

In this paper, we explore other possible guests and processing conditions leading to the formation of high-SA NC PPO films. In this framework, we found crystallization conditions that lead to high SA (with SA up to 450 $m^2\ g^{-1}$) with transparency and toughness comparable with those of NC PPO films, exhibiting negligible SA.

Dipartimento di Chimica e Biologia "A. Zambelli" and INSTM Research Unit, Università degli Studi di Salerno, Via Giovanni Paolo II, 132, 84084 Fisciano (SA), Italy. E-mail: bakunagendra@gmail.com, gguerra@unisa.it

Experimental section

Materials and sample preparation

Poly(2,6-dimethyl-1,4-phenylene) oxide with M_w = 350 kg mol^{-1} (Ultra High P6130 grade) was supplied by Sabic, the Netherlands. Toluene, methyl benzoate, 1,3,5-trimethylbenzene (mesitylene), carvone, limonene, eugenol, carvacrol, dibenzyl ether, chloroform ($CHCl_3$), acetonitrile (ACN), perchloroethylene (PCE), methanol, and $CaCl_2$ were purchased from Sigma-Aldrich, Italy.

Amorphous film preparation

Amorphous PPO films with 20–200 μm thickness were obtained by casting 0.1–1 wt% $CHCl_3$ solution at T = 60 °C. $CHCl_3$ was extracted from the cast amorphous PPO films by ACN guest sorption/desorption at room temperature.

Table 1 The BET surface area (m^2 g^{-1}) and degree of crystallinity (%) of NC PPO films obtained by liquid phase guest-induced crystallization of amorphous PPO films (≈20 microns) at different temperatures. Guest molecules are ordered based on their diffusivities in amorphous PPO films (D, cm^2 sec^{-1}) at room temperature

		Liquid phase guest-induced crystallization temperature (°C)					
		4 °C		30 °C		65 °C	
Guest molecule	Guest diffusivity (D) at rt (cm^2 s^{-1})	BET surface area (m^2 g^{-1})	Crystallinity (%)	BET surface area (m^2 g^{-1})	Crystallinity (%)	BET surface area (m^2 g^{-1})	Crystallinity (%)
Toluene	High	185	43	Film dissolution			
Mesitylene	1.9×10^{-9}	175	45	165	44	Film dissolution	
Dibenzyl ether	9.8×10^{-10}	Negligible	38	560	46	Film dissolution	
Carvone	4.4×10^{-10}	Negligible	40	620	44	Film dissolution	
Limonene	5.5×10^{-11}	Negligible	19	Negligible	33	490	54
Eugenol	2.6×10^{-11}	Negligible	18	Negligible	33	440	56
Carvacrol	6.4×10^{-12}	Negligible	10	Negligible	24	330	48

Guest-induced crystallization

Liquid guest-induced crystallization. Liquid guest-induced crystallization of amorphous PPO films (20–100 μm) was conducted by sorption of liquids at temperatures in the range of 4–80 °C (Table 1).[47]

Vapor guest-induced crystallization. Vapor guest-induced crystallization was studied for the guest molecules listed in Table 2. Typically, the vapor phase guest-induced crystallization was conducted by laying amorphous PPO films (20–100 μm) on the surface of the liquid guest for 5–15 minutes at a temperature close to the guest boiling point.

Guest removal from the CC films was conducted by supercritical carbon dioxide ($scCO_2$) extraction. General extraction conditions comprised temperature = 40 °C, pressure = 250 bar, and time = 4 hours. The thickness of amorphous films after full guest removal increased by a factor of 2.1–2.2 and 2.9–3.3 for liquid-induced crystallization at 4 °C and room temperature, respectively. An intermediate increase of thickness (factor in the range 2.4–2.7) was observed for vapor-induced crystallization (with carvone at 220 °C).

Characterization techniques

Wide-angle X-ray diffraction (WAXD) patterns were collected with a Bruker D8 diffractometer (at an operating step size of 0.03° and a rate of 0.2 s/step with nickel-filtered Cu Kα radiation). Two-dimensional wide-angle X-ray diffraction (2D-WAXD) patterns obtained by sending the X-ray beam parallel or perpendicular to the film surface are called EDGE or THROUGH patterns in the discussion onwards. The degree of planar orientation (f_c) of the PPO films was evaluated by using Hermans' orientation function:

$$f_c = \left(3\overline{\cos^2\gamma} - 1\right)/2 \quad (1)$$

where $\cos^2\gamma$ is determined by the azimuthal distribution of 001 reflection intensity for the 2D-WAXD EDGE patterns. When $f_c(001)$ is equal to −0.5 or 1, the c axes of all crystallites are perfectly perpendicular or parallel to the film plane, respectively. When $f_c(001)$ is equal to 0, a random crystallite orientation occurs.

The correlation length of the crystalline domains was evaluated for the intense and rather isolated 210 equatorial reflections, which were located at a diffraction angle of $2\theta = 11.2°$ by using the Scherrer's formula:

$$D_{210} = (k\lambda)/(\beta \cos\theta_{210}) \quad (2)$$

where λ is the wavelength of the X-ray (0.154 nm); k is the shape factor assumed to be 0.9; β is the full width at half-maximum (FWHM) of the 210 reflections as taken from radial profiles of 2D-WAXD THROUGH patterns.

Nitrogen adsorption measurements were performed at 77 K on a Nova Quantachrome 4200e instrument. The specific SA of the NC PPO films was calculated using the Brunauer–Emmett–Teller (BET) method in the $0.05 < p/p_0 < 0.2$ pressure range. The surface morphology of the PPO films was analyzed by scanning electron microscopy (Carl Zeiss SMT AG, Oberkochen, Germany). Before imaging, all PPO film samples were coated with gold (Agar Auto Sputter Coater model 108 A, Stansted, UK) at 30 mA for 5 min. Thermogravimetric analysis (TGA, TA Q500 equipment) was used to quantify the guest content in the co-crystalline PPO films.

Differential scanning calorimetry (DSC, TA Q2000 equipment) was used to measure the melting enthalpies of the NC PPO films. The heating and cooling cycles were conducted at a rate of 10 °C min^{-1}. Degrees of crystallinity (X_c) of NC PPO films were estimated based on the following equation:

$$X_c = \frac{\Delta H_f}{\Delta H_f^\circ} \quad (3)$$

Table 2 The BET surface area (m^2 g^{-1}) and degree of crystallinity (%) of NC PPO films obtained by vapor phase guest-induced crystallization of amorphous PPO films (≈20 microns) at temperatures close to the guest boiling point. Guest molecules are ordered based on their boiling temperatures (2nd column)

Guest molecule	Boiling point (°C)	BET surface area (m^2 g^{-1})	Degree of crystallinity (%)
Toluene	110	Film dissolution	
Mesitylene	164	325	44
Limonene	176	170	35
Carvone	231	450	56
Carvacrol	237	305	47
Eugenol	254	205	51
Dibenzyl ether	298	T_b (guest) > T_m (polymer host)	

Where ΔH_f and ΔH°_f are melting enthalpies of semicrystalline and fully crystalline PPO samples, respectively. The melting enthalpy of the fully crystalline PPO samples is assumed as 42 ± 2 J g^{-1}.[50]

Because the high-SA films exhibit macroporosity, their densities cannot be evaluated by the standard floatation method (generally conducted in aqueous solutions of methanol or $CaCl_2$). For this reason, the density of our films (ρ) was simply obtained as the mass/volume ratio of rectangular homogeneous samples. We verified that the two film density evaluation methods lead to close values, both for amorphous (1.04 g cm^{-3}) and for NC $c\perp$ oriented (0.98 g cm^{-3}) films.

The density of the polymer (ρ_p) that is present in the high-SA films was calculated based on the degree of crystallinity (X_c, obtained from DSC) and of the density of amorphous PPO (ρ_{am} = 1.04 g cm^{-3}) and the NC α-form (ρ_α = 0.93 g cm^{-3}), by using the formula:[20]

$$\rho_p = \rho_\alpha X_c + \rho_{am}(1 - X_c) \quad (4)$$

The porosity (P) of NC films was evaluated as follows:

$$P = 100\left[1 - \frac{\rho}{\rho_p}\right] \quad (5)$$

Vapor sorption measurements ($0.05 \geq p/p_0 \geq 0.01$) were performed at 35 °C with a VTI-SA symmetrical vapor sorption analyzer (TA instruments). The diffusion coefficient (D) of PCE in PPO films was evaluated based on the following equation:

$$\frac{d\left(\frac{M_t}{M_\infty}\right)}{d\left(t^{\frac{1}{2}}\right)} = \left(16D/L^2\pi\right)^{1/2} \quad (6)$$

where L is the film thickness, while M_t and M_∞ are the masses of PCE absorbed at the time t at equilibrium, respectively.

Results and discussion

Liquid guest-induced crystallization

The known procedure of guest-induced crystallization leading to high-SA NC PPO films requires fast crystallization of amorphous films induced by high uptake of non-volatile guests, followed by a guest exchange with a volatile guest.[48] The literature data refer to the sorption of liquid carvone and dibenzyl ether at room temperature.[48] This procedure is now extended to lower (4 °C) and higher (65 °C) temperatures and to other non-volatile guests of CC phases of PPO (*e.g.*, toluene, mesitylene, limonene, eugenol, and carvacrol). The BET SA and the degree of crystallinity (as evaluated by DSC measurements) of the obtained films are summarized in Table 1, where the guests are ordered based on their room temperature diffusivities in amorphous PPO films (2nd column).

From Table 1, it is apparent that the highly diffusive toluene guest leads to high-SA NC films only at low sorption temperatures, while it dissolves amorphous PPO films at 30 °C and 65 °C. Mesitylene leads to high-SA NC films for sorption at 4 °C and 30 °C, while it dissolves amorphous PPO films at 65 °C. Dibenzyl ether and carvone have a similar behavior: both lead to high-SA NC films for sorption at 30 °C, while they dissolve amorphous PPO films at 65 °C. Moreover, both guests when absorbed at 4 °C led to low SA NC films due to very slow guest sorption (and guest-induced crystallization) kinetics.[48,49] The three guests presented in Table 1 with the lowest diffusivities (limonene, eugenol, and carvacrol) lead to high-SA NC films only at the highest sorption temperature (65 °C). Guest-sorption procedures conducted at lower temperatures lead to low-SA NC films, with $c_\perp$ orientations.[44–47]

In summary, the results presented in Table 1 indicate that non-volatile guests of CC phases of PPO can give high-SA NC PPO films, provided that suitable guest sorption temperatures are chosen. It is necessary to avoid very high sorption kinetics, which may lead to the dissolution of amorphous PPO films (upper right part of Table 1), as well as very low sorption kinetics, which may lead to low-SA NC PPO films (lower left part of Table 1).

Vapor guest-induced crystallization

In this section, guest-induced crystallization of PPO amorphous films is explored for the guests in Table 1 by using high-temperature vapors rather than low-temperature liquids. Our experiments on vapor-induced crystallization were conducted by exposing amorphous PPO films to vapors at temperatures close to the guest boiling point (2nd column in Table 2).

This new route to get high-SA NC PPO films was effective with most of the guests assessed here. It was not only effective for toluene, which is a very strong solvent for PPO (first line of Table 2), and for dibenzyl ether, whose boiling point (as well as treatment temperature) was higher than the melting temperature of PPO[51–54] (last row in Table 2). For the other entries in Table 2, the guest content after the vapor sorption procedure was in the range of 65–80 wt% and became null after the acetonitrile sorption/desorption procedure.

The most relevant feature of the high-SA NC PPO films presented in Table 2 (that were obtained by vapor guest-induced crystallization) was that they were all transparent and tough, whereas all the high-SA NC PPO films in Table 1 obtained by liquid guest-induced crystallization, were opaque and brittle.

A comparison of structure, morphology, transparency, toughness, and guest uptake of high-SA NC PPO films obtained by liquid or vapor guest-induced crystallization, is presented in the next three sections.

Structure and morphology of high-surface area NC PPO Films

In this section, as well as in the next two sections, a comparison between three NC PPO films with similar thickness is presented ($\approx$50 μm): (i) a transparent high-SA obtained by vapor guest-induced crystallization (red lines); (ii) an opaque high-SA obtained by liquid guest-induced crystallization (blue lines); and (iii) a highly diffusive low SA with $c_\perp$ orientation (black lines). The main quantitative results are summarized in Table 3.

Table 3 Characterization of NC PPO α-form films obtained by carvone-induced crystallization of amorphous films: (2nd row) transparent high-SA NC PPO film by vapor induced crystallization; (3rd row) opaque high-SA NC PPO by liquid induced crystallization; (4th row) $c_\perp$ NC PPO by low-temperature liquid induced crystallization; (5th row) amorphous PPO. Correlation length (D_{210}, nm), degree of crystallinity (X_c, %, by DSC), measured film density (ρ, g cm^{-3}), percent of porosity (P), crystallite size based on SEM images (nm), BET surface area (m^2 g^{-1}), light transmittance at 600 nm (%), PCE diffusivity at 35 °C and p/p_0 = 0.01 (D, cm^2 s^{-1})

PPO film	D_{210} (nm)	Degree of crystallinity (%)	Density (ρ, g cm^{-3})	% of porosity based on the density (%)	Crystallite sizes based on SEM images (nm)	BET surface area (m^2 g^{-1})	Transmittance at 600 nm (%)	PCE diffusivity at 35 °C, p/p_0 = 0.01 (cm^2 s^{-1})
Transparent high-SA NC film	5.6	56	0.91	7	40–60	450	74	2.8×10^{-9}
Opaque high-SA NC film	5.4	45	0.82	16.5	40–60	620	0	3.3×10^{-9}
$c_\perp$ NC film	5.5	40	0.98	0	35–45	<4	86	6.6×10^{-10}
Amorphous film	—	0	1.04	0	—	<4	90	8.2×10^{-12}

The WAXD patterns (in particular, radial profiles of 2D THROUGH patterns) of the three films are shown in Fig. 1. All these patterns show intense equatorial 100, 010, 210, and 310 reflections that are typical of the NC α-form.[20,22] The broadness of these diffraction peaks, being similar for the three films considered here, indicates the occurrence of similar correlation lengths of the polymer crystallites. For instance, the correlation length as calculated for the intense and rather isolated 210 reflections (D_{210}) is in the narrow range of 5.4–5.6 nm.

The degree of crystallinity of these films cannot be easily compared by WAXD patterns due to the occurrence of $c_\perp$ orientation in the film (Fig. 1c). The degree of crystallinity of these films can instead be safely evaluated by melting enthalpies obtained from the DSC scans.[50] The DSC scans of the three films at a heating rate of 10 °C min^{-1} have been compared in Fig. 2, where the melting enthalpies and melting temperatures are also indicated.

The transparent film from vapor carvone-induced crystallization exhibits melting enthalpy (and the related degree of crystallinity, $X_c \approx 56\%$) and melting temperature ($T_m \approx 262$ °C) much higher than for the other two films ($40\% < X_c < 45\%$ and 242 °C $< T_m <$ 245 °C). This indicates that the crystallization of amorphous PPO films induced by high-temperature vapor guest sorption not only leads to higher degrees of crystallinity but also to higher crystalline phase perfection.

The measured film densities (ρ) are compared in the 4th column of Table 3. Film porosity calculated based on these density values by using eqn (4) is reported in the 5th column of Table 3. The porosity of the vapor guest crystallized film was much lower than that of the liquid guest crystallized film (at 4 °C).

The SEM images of the three films at different magnifications are compared in Fig. 3(a–c) and (a′–c′). Macroporosity was observed in the film crystallized by sorption of liquid carvone at

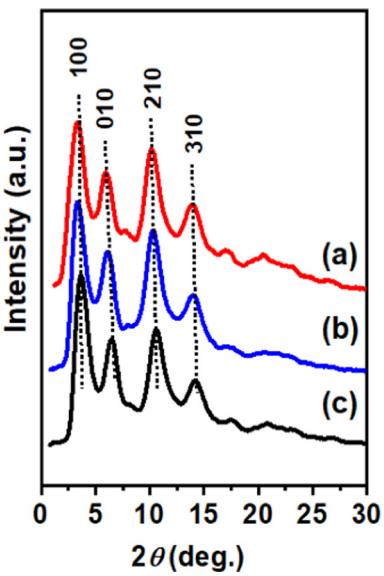

Fig. 1 Radial profiles of 2D-WAXD THROUGH patterns of NC PPO films obtained by guest extraction from CC PPO films: (a) high-SA transparent (from vapor phase carvone-induced crystallization); (b) high-SA opaque (from liquid phase carvone-induced crystallization at 30 °C); and (c) low SA transparent $c_\perp$ oriented (from liquid phase carvone-induced crystallization at 4 °C).

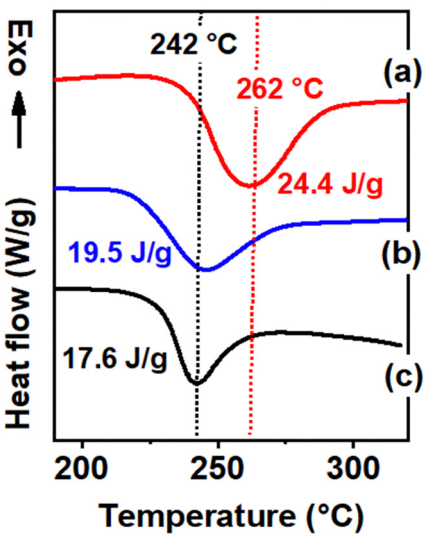

Fig. 2 The DSC scans of NC PPO films obtained by carvone-induced crystallization: (a) vapor guest sorption; (b) liquid guest sorption at 30 °C, and (c) liquid guest sorption at 4 °C. Melting enthalpies and temperatures are indicated close to the curves.

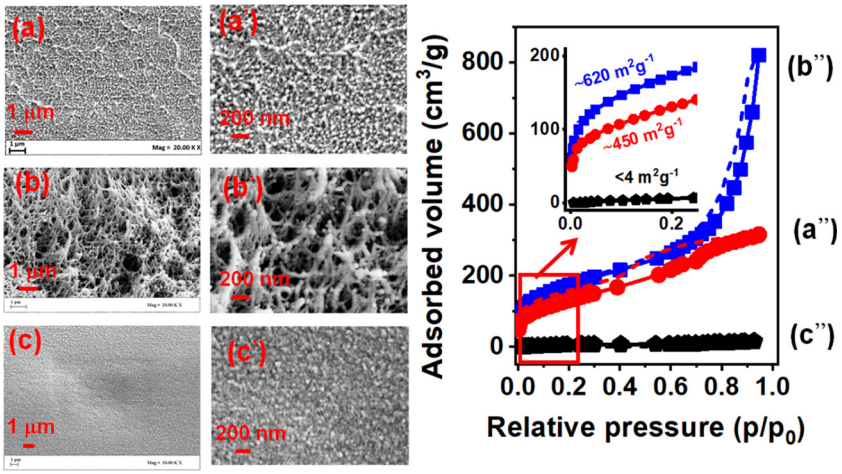

Fig. 3 (a–c and a′–c′) SEM images with different magnifications and (a″–c″) volumetric N_2 adsorption/desorption isotherms measured at 77 K for the NC PPO films, whose crystallization was induced by carvone sorption: (a and a′) from vapor phase; (b and b′) from the liquid phase at room temperature; (c and c′) from the liquid phase at 4 °C. Thick and dotted isotherms represent adsorption and desorption curves, respectively. The inset shows the enlarged low-pressure adsorption curves with the BET SA.

room temperature (Fig. 3b and b′), while no macroporosity were observed in the film crystallized by sorption of carvone vapor (Fig. 3a and a′).

N_2 sorption isotherms measured at 77 K for the three NC films are shown in Fig. 3(a″–c″). The sorption behavior observed for $p/p_0 < 0.2$, which is shown as an inset in Fig. 3, is particularly interesting. The BET SA of the transparent (and highly diffusive)[48] $c_\perp$ oriented film that was obtained from liquid carvone-induced crystallization at 4 °C was negligible (Fig. 3c″), while the BET SA of the opaque film that was obtained from liquid carvone-induced crystallization at room temperature was very high (Fig. 3b″, 620 $m^2\ g^{-1}$). Surprisingly, the BET SA of the transparent film, from vapor-induced crystallization at the carvone boiling point, was quite high (Fig. 3a″, 450 $m^2\ g^{-1}$).

Transparency and toughness of high-surface area NC PPO films

All the high-SA films of Table 1, as those described in ref. 48 and 49, were completely opaque. Their density was always in the range of 0.80–0.85 g cm^{-3}, *i.e.*, also lower than for the NC α-form (0.93 g cm^{-3}), clearly indicating the presence of a large number of voids (20–10 vol%) in the semi-crystalline films. The occurrence of large amounts of macropores, which were apparent in the SEM images shown in Fig. 3b and b′, was confirmed by optical and mechanical characterizations of the films.

Digital photos of films laying on the monomer unit chemical formula of PPO are shown in Fig. 4. As expected, the highest transparency occurs for the fully amorphous film (Fig. 4d), while slightly reduced transparency was observed for the NC film with $c\perp$ orientation (Fig. 4c),[55] as well as for the NC film, crystallized by carvone sorption from the vapor phase (Fig. 4a).

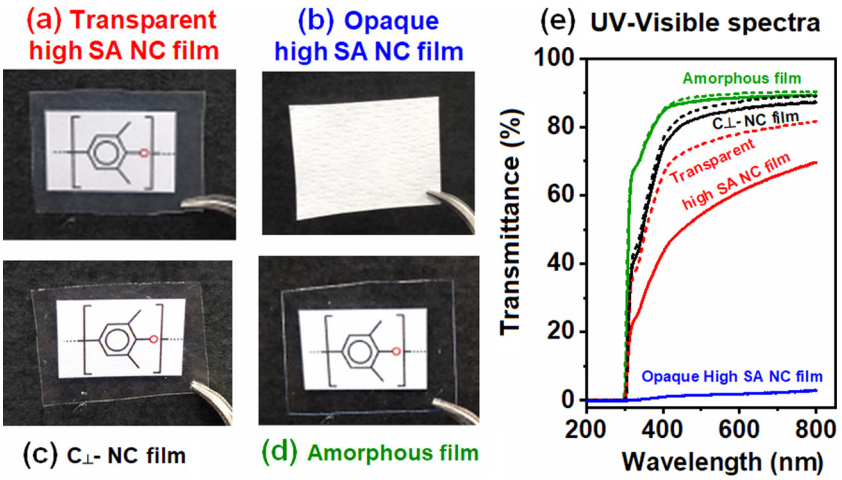

Fig. 4 (a–d) Digital photos of PPO films with a thickness of ~50 μm. To show possible transparency, the molecular formula of PPO is laying below the film. (a–c) NC obtained by carvone-induced crystallization: (a) from the vapor phase (red label and curves); (b) from the liquid phase at room temperature (blue label and curves); (c) from the liquid phase at 4 °C (black label and curves). (d) amorphous (green label and curves). (e) UV-Visible spectra of (a–d) PPO films. Dashed and continuous lines indicate transmittance for films with thicknesses of ≈50 μm and ≈100 μm, respectively.

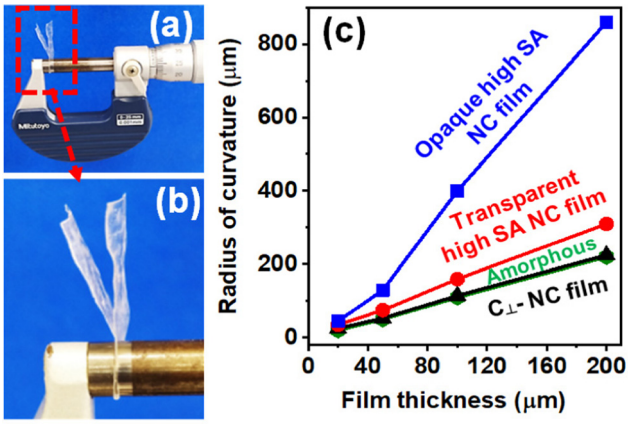

Fig. 5 (a and b) Digital Photos of the used bending test for PPO films that evaluated the minimum opening of a gauge before film breaking. (c) The radius of curvature (one-half of this minimum opening) *versus* thickness of PPO films: (blue squares) opaque high-SA NC, (red circles) transparent high-SA NC, (black triangles) $c_\perp$ NC, and (green pentagons) amorphous.

NC films crystallized at room temperature by liquid carvone sorption were completely opaque (Fig. 4b). This information was quantified by UV-Visible spectra for films with a thickness of nearly 50 μm and 100 μm (Fig. 4e).

The toughness of films, such as those listed in Table 3 (and shown in Fig. 4), was explored by bending tests, which evaluated the opening of a gauge at film breaking, as shown by digital photos in Fig. 5a and b.

Fig. 5c shows the radius of curvature leading to film breaking (one-half of the minimum gauge opening) *versus* the film thickness. It is apparent that the transparent high-SA NC PPO films (from the vapor-induced crystallization) exhibit a strongly reduced brittleness as compared to the opaque high-SA NC PPO films (from liquid-induced crystallization), which was comparable to that of amorphous PPO films and the $c_\perp$ NC PPO films.

Guest sorption kinetics from high-surface area NC PPO films

Guest diffusivities in PPO films of the four kinds listed in Table 3 were studied by guest sorption kinetics at low vapor pressures. As an example, the sorption kinetics of a relevant chlorinated pollutant (perchloroethylene, PCE)[56–59] at 35 °C at a low relative pressure (p/p_0 = 0.01) are shown in Fig. 6a.

Amorphous PPO films, although well known for their high free-volume and molecular uptake,[60–64] exhibit guest uptake much smaller and slower than for the NC film with $c_\perp$ orientation[44] and enormously smaller and slower than for the known opaque high-SA NC films.[48]

The most relevant result of Fig. 6a is that the new high-SA NC film obtained by vapor-induced crystallization, which has transparency and toughness comparable with those of amorphous PPO films, has guest uptake kinetics comparable with those of the already known opaque and brittle high-SA films. More interestingly, the new high-SA NC PPO films also have higher guest uptakes at equilibrium, if measured as weight uptake per unit volume (Fig. 6b), *i.e.*, the amount that matters for most practical applications.

Conclusions

NC PPO films with transparency and toughness close to those of amorphous PPO films, as well as a surface area of up to 450 $m^2\ g^{-1}$ and organic guest diffusivity comparable to those of opaque high-SA NC PPO films and aerogels, are presented. These high-SA polymer films have transparency and toughness close to those of NC PPO films with $c_\perp$ orientation (*i.e.* the chain axes of the crystalline phase are preferentially perpendicular to the film plane) but with much higher SA and faster guest sorption kinetics. These new high-SA dense and transparent polymer films are unprecedented and can be even achieved with a high thickness (of at least up to 100 μm).

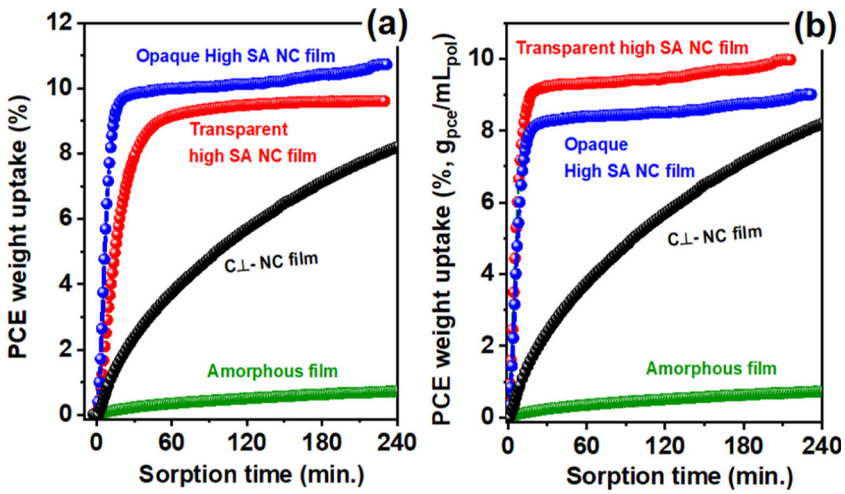

Fig. 6 PCE sorption kinetics for p/p_0 = 0.01 at 35 °C measured for different PPO films: (red circles) transparent high-SA NC; (blue circles) opaque high-SA NC; (black circles) c⊥ NC; (green circles) amorphous. PCE uptake is expressed as the mass of guest per mass of the polymer (a) or as the mass of guest per volume of polymer (b).

Preparation procedures leading to transparent and tough high-SA films require (i) guest-induced co-crystallization by large uptake (typically 60–80 wt%) of a highly boiling guest molecule (*e.g.*, mesitylene, limonene, carvone, carvacrol, eugenol) in amorphous PPO films; (ii) guest sorption from vapor phase at a temperature close to the guest boiling point; and (iii) subsequent guest removal by sorption/desorption of a volatile guest, leading to the formation of NC phases.

These high-SA, transparent, and tough NC PPO films are expected to be suitable for many applications, mainly for organic pollution remediation, molecular separation, and molecular sensing. Many applications are also expected for the corresponding films exhibiting CC phases obtained by the sorption of functional guest molecules. Transparency, of course, is particularly relevant for CC films for guests with optical properties (chromophore, fluorescent, photoreactive, and chiral-optical).

Author contributions

The manuscript was written with the contributions of all authors. All authors have approved the final version of the manuscript.

Conflicts of interest

The authors declare no competing interests.

Acknowledgements

Financial support of Ministero dell'Università e della Ricerca (MUR, 0179BJNA2; Prin2020, 2020EZ8EPB) is gratefully acknowledged.

References

1 J. M. Barrales-Rienda and J. M. G. Fatou, Single crystals of poly(2,6-dimethyl-1,4-phenylene) oxide, *Colloid Polym. Sci.*, 1971, **244**, 317–323.
2 S. Horikiri, Single crystals of poly(2,6-dimethylphenylene oxide), *J. Polym. Sci., Polym. Phys. Ed.*, 1972, **10**, 1167–1170.
3 J. Hurek and E. Turska, X-ray studies of crystallization of poly(2,6-dimethyl-1,4-phenylene oxide) on swelling in certain systems, *Acta Polym.*, 1984, **35**, 201–207.
4 O. Tarallo, V. Petraccone, C. Daniel, G. Fasano, P. Rizzo and G. Guerra, A chiral co-crystalline form of poly(2,6-dimethyl-1,4-phenylene)oxide (PPO), *J. Mater. Chem.*, 2012, **22**, 11672–11680.
5 P. Rizzo, G. Ianniello, L. Longo and G. Guerra, Uniplanar orientations and guest exchange in PPO co-crystalline films, *Macromolecules*, 2013, **46**, 3995–4001.
6 M. Golla, B. Nagendra, C. Daniel, P. Rizzo and G. Guerra, Isolated and aggregated carvacrol guest molecules in cocrystalline poly(2,6-dimethyl-1,4-phenylene)oxide films, *Polym. J.*, 2021, **53**, 1093–1100.
7 G. Guerra, C. Daniel, P. Rizzo and O. Tarallo, Advanced materials based on polymer cocrystalline forms, *J. Polym. Sci., Part B: Polym. Phys.*, 2012, **50**, 305–322.
8 Y. Chatani, T. Inagaki, Y. Shimane and H. Shikuma, Structural study on syndiotactic polystyrene: 4. Formation and crystal structure of molecular compound with iodine, *Polymer*, 1993, **34**, 4841–4845.
9 Y. Chatani, Y. Shimane, T. Inagaki, T. Ijitsu, T. Yukinari and H. Shikuma, Structural study on syndiotactic polystyrene: 2. Crystal structure of molecular compound with toluene, *Polymer*, 1993, **34**, 1620–1624.
10 E. Bhoje Gowd, S. S. Nair and C. Ramesh, Crystalline Transitions of the Clathrate (δ) Form of Syndiotactic Polystyrene during Heating: Studies Using High-Temperature X-ray Diffraction, *Macromolecules*, 2002, **35**, 8509–8514.
11 V. Venditto, G. Milano, A. De Girolamo Del Mauro, G. Guerra and J. Mochizuki, Itagaki, Orientation and microenvironment of naphthalene guest in the host nanoporous phase of syndiotactic polystyrene, *Macromolecules*, 2005, **38**, 3696–3702.
12 Y. Uda, F. Kaneko, N. Tanigaki and T. Kawaguchi, The first example of a polymer-crystal-organic-dye composite material: The clathrate phase of syndiotactic polystyrene with azulene, *Adv. Mater.*, 2005, **17**, 1846–1850.
13 C. Daniel, N. Galdi, T. Montefusco and G. Guerra, Syndiotactic polystyrene clathrates with polar guest molecules, *Chem. Mater.*, 2007, **19**, 3302–3308.
14 A. R. Albunia, C. D'Aniello, G. Guerra, D. Gatteschi, M. Mannini and L. Sorace, Ordering magnetic molecules within nanoporous crystalline polymers, *Chem. Mater.*, 2009, **21**, 4750–4752.
15 O. Tarallo, V. Petraccone, A. R. Albunia, C. Daniel and G. Guerra, Monoclinic and triclinic δ -clathrates of syndiotactic polystyrene, *Macromolecules*, 2012, **43**, 8549–8558.
16 O. Tarallo, M. M. Schiavone, V. Petraccone, C. Daniel, P. Rizzo and G. Guerra, Channel clathrate of syndiotactic polystyrene with *p*-nitroaniline, *Macromolecules*, 2010, **43**, 1455–1466.
17 T. Sano, A. Uchiyama, T. Sago and H. Itagaki, Fluorescence behavior of syndiotactic polystyrene and its derivative: Formation of a ground-state dimer in the solid state, *Eur. Polym. J.*, 2017, **90**, 114–121.
18 A. Cozzolino, G. Monaco, C. Daniel, P. Rizzo and G. Guerra, Monomeric and dimeric carboxylic acid in crystalline cavities and channels of delta and epsilon forms of syndiotactic polystyrene, *Polymers*, 2021, **13**, 3330.
19 C. Daniel, S. Longo, G. Fasano, J. G. Vitillo and G. Guerra, Nanoporous crystalline phases of poly(2,6-dimethyl-1,4-phenylene)oxide, *Chem. Mater.*, 2011, **23**, 3195–3200.
20 M. Galizia, C. Daniel, G. Fasano, G. Guerra and G. Mensitieri, Gas sorption and diffusion in amorphous and semicrystalline nanoporous poly(2,6-dimethyl-1,4-phenylene)-oxide, *Macromolecules*, 2012, **45**, 3604–3615.
21 C. Daniel, D. Zhovner and G. Guerra, Thermal stability of nanoporous crystalline and amorphous phases of poly(2,6-dimethyl-1,4-phenylene)oxide, *Macromolecules*, 2013, **46**, 449–454.

22 B. Nagendra, A. Cozzolino, C. Daniel, P. Rizzo, G. Guerra, F. Auriemma, C. De Rosa, M. C. D'Alterio, O. Tarallo and A. Nuzzo, Two nanoporous crystalline forms of poly(2,6-dimethyl-1,4-phenylene)oxide and related co-crystalline forms, *Macromolecules*, 2019, **52**, 9646–9656.
23 M. Golla, B. Nagendra, C. Daniel, P. Rizzo, F. Auriemma, O. Tarallo and G. Guerra, Intrahelical empty channels of nanoporous-crystalline α and β forms of PPO, *Eur. Polym. J.*, 2022, **179**, 111568.
24 F. Auriemma, C. Daniel, M. Golla, B. Nagendra, P. Rizzo, O. Tarallo and G. Guerra, Polymorphism of poly(2,6-dimethyl-1,4-phenylene) oxide (PPO): co-crystalline and nanoporous-crystalline phases, *Polymer*, 2022, **258**, 125290.
25 A. Yu Alentiev, I. S. Levin, M. I. Buzin, N. A. Belov, R. Yu Nikiforov, S. V. Chirkov, I. V. Blagodatskikh, A. S. Kechekyan, P. A. Kechekyan, V. G. Bekeshev, V. E. Ryzhikh, P. Yu and P. Yampolskii, Gas transport parameters, density and free volume of nanocrystalline poly-2,6-dimethylphenylene oxide, *Polymer*, 2021, **226**, 123804.
26 A. Y. Alentiev, I. S. Levin, N. A. Belov, R. Y. Nikiforov, S. V. Chirkov, D. A. Bezgin, V. E. Ryzhikh, J. V. Kostina, V. P. Shantarovich and L.-Y. Grunin, Features of the gas-permeable crystalline phase of poly-2,6-dimethylphenylene oxide, *Polymers*, 2022, **14**, 120.
27 C. De Rosa, G. Guerra, V. Petraccone and B. Pirozzi, Crystal structure of the emptied clathrate form (δ_e form) of syndiotactic polystyrene, *Macromolecules*, 1997, **30**, 4147–4152.
28 Y. Uda, F. Kaneko and T. Kawaguchi, Selective guest uptake from solvent mixtures in the clathrate phase of syndiotactic polystyrene, *Macromol. Rapid Commun.*, 2004, **25**, 1900–1904.
29 M. M. Sivakumar, T. Suzuki, Y. Yamamoto, K. P. O. Mahesh, H. Yoshimizu and Y. Tsujita, Structure and properties of the mesophase of syndiotactic polystyrene, *J. Membr. Sci.*, 2005, **262**, 11–19.
30 S. Malik, D. Roizard and J.-M. Guenet, Multiporous material from fibrillar syndiotactic polystyrene intercalates, *Macromolecules*, 2006, **39**, 5957–5959.
31 V. Petraccone, O. Ruiz de Ballesteros, O. Tarallo, P. Rizzo and G. Guerra, Nanoporous polymer crystals with cavities and channels, *Chem. Mater.*, 2008, **20**, 3663–3668.
32 B. Bhoje Gowd, K. Tashiro and C. Ramesh, Structural phase transitions of syndiotactic polystyrene, *Prog. Polym. Sci.*, 2009, **34**, 280–315.
33 C. Daniel, P. Antico and G. Guerra, Etched fibers of syndiotactic polystyrene with nanoporous-crystalline phases, *Macromolecules*, 2018, **51**, 6138–6148.
34 Y. Tamai, Effective and efficient transport mechanism of CO_2 in subnano-porous crystalline membrane of syndiotactic polystyrene, *J. Membr. Sci.*, 2022, **646**, 120202.
35 C. Daniel, L. Longo, S. Cardea, J. G. Vitillo and G. Guerra, Monolithic nanoporous–crystalline aerogels based on PPO, *RSC Adv.*, 2012, **2**, 12011–12018.
36 C. Daniel, M. Pellegrino, V. Venditto, S. Aurucci and G. Guerra, Nanoporous-crystalline poly(2,6-dimethyl-1,4-phenylene)oxide (PPO) aerogels, *Polymer*, 2016, **105**, 96–103.
37 C. Daniel, S. Longo, R. Ricciardi, E. Reverchon and G. Guerra, Monolithic nanoporous crystalline aerogels, *Macromol. Rapid Commun.*, 2013, **34**, 1194–1207.
38 C. Daniel, D. Alfano, V. Venditto, S. Cardea, E. Reverchon, D. Larobina, G. Mensitieri and G. Guerra, Aerogels with a microporous crystalline host phase, *Adv. Mater.*, 2005, **17**, 1515–1518.
39 C. D'Aniello, C. Daniel and G. Guerra, ε Form gels and aerogels of syndiotactic polystyrene, *Macromolecules*, 2015, **48**, 1187–1193.
40 X. Wang and S. C. Jana, Synergistic Hybrid Organic-Inorganic Aerogels, *ACS Appl. Mater. Interfaces*, 2013, **5**, 6423–6429.
41 X. Wang and S. C. Jana, Syndiotactic polystyrene aerogels containing multi-walled carbon nanotubes, *Polymer*, 2013, **54**, 750–759.
42 P. Raut, W. Liang, Y.-M. Chen, Y. Zhu and S. C. Jana, Syndiotactic Polystyrene-Based Ionogel Membranes for High-Temperature Electrochemical Applications, *ACS Appl. Mater. Interfaces*, 2017, **9**, 30933–30942.
43 V. G. Krishnan, A. M. Joseph, S. K. Peethambharan and E. Bhoje Gowd, Nanoporous Crystalline Aerogels of Syndiotactic Polystyrene: Polymorphism, Dielectric, Thermal, and Acoustic Properties, *Macromolecules*, 2021, **54**, 10605–10615.
44 A. Kulkarni and S. C. Jana, Surfactant-free syndiotactic polystyrene aerogel foams via Pickering emulsion, *Polymer*, 2021, **212**, 123125.
45 C. Daniel, P. Rizzo, B. Nagendra, A. Cozzolino and G. Guerra, High diffusivity dense films of a nanoporous-crystalline polymer, *Polymer*, 2021, **229**, 124005.
46 A. Cozzolino, B. Nagendra, P. Rizzo, C. Daniel and G. Guerra, Fast uptake of organic pollutants from dilute aqueous solutions by nanoporous-crystalline PPO films with c-perpendicular orientation, *Eur. Polym. J.*, 2021, **161**, 110864.
47 P. Rizzo, C. Gallo, V. Vitale, O. Tarallo and G. Guerra, Nanoporous-crystalline films of PPO with parallel and perpendicular polymer chain orientations, *Polymer*, 2019, **167**, 193–201.
48 B. Nagendra, M. Golla, C. Gallo, C. Daniel, P. Rizzo, G. Guerra, L. Baldino and E. Reverchon, Mechanisms determining different planar orientations in PPO films crystallized by guest sorption, *Polymer*, 2021, **235**, 24242.
49 B. Nagendra, A. Cozzolino, C. Daniel, P. Rizzo and G. Guerra, High surface area nanoporous-crystalline polymer films, *Macromolecules*, 2022, **55**, 2983–2990.
50 B. Nagendra, C. Daniel, P. Rizzo, G. Guerra, L. Baldino and E. Reverchon, High surface area polymer films by co-crystallization with low-molecular-mass guest molecules, *Eur. Polym. J.*, 2022, **173**, 111305.
51 B. Nagendra, E. Vignola, C. Daniel, P. Rizzo and G. Guerra, Dependence on Film Thickness of Guest-Induced *c* Perpendicular Orientation in PPO Films, *Polymers*, 2021, **13**, 4384.
52 F. E. Karasz and J. M. O'Reilly, Thermal properties of poly(2,6-dimethylphenylene ether), *J. Polym. Sci. B Polym. Lett.*, 1965, **3**, 561–563.

53 S. Z. D. Cheng and B. Wunderlich, Glass transition and melting behavior of poly(oxy-2,6-dimethyl-1,4-phenylene), *Macromolecules*, 1987, **20**, 1630–1637.
54 B. Nagendra, M. Golla, C. Daniel, P. Rizzo and G. Guerra, Melting of nanoporous-crystalline and co-crystalline solution cast films of poly(2,6-dimethyl-1,4-phenylene) oxide, *Polymer*, 2021, **228**, 123935.
55 B. Nagendra, P. Rizzo, C. Daniel and G. Guerra, Planar Orientation and Transparency of Nanoporous-Crystalline Polymer Films, *Macromolecules*, 2021, **54**, 6605–6611.
56 D. L. Freedman and J. M. Gossett, Biological reductive dechlorination of tetrachloroethylene and trichloroethylene to ethylene under methanogenic conditions, *Appl. Environ. Microbiol.*, 1989, **55**, 2144–2151.
57 G. Chen, Reductive dehalogenation of tetrachloroethylene by microorganisms: current knowledge and application strategies, *Appl. Microbiol. Biotechnol.*, 2004, **63**, 373–377.
58 J. A. Cichocki, K. Z. Guyton, N. Guha, W. A. Chiu, I. Rusyn and L. H. Lash, Target organ metabolism, toxicity, and mechanisms of trichloroethylene and perchloroethylene: key similarities, differences, and data gaps, *J. Pharm. Exper. Therap.*, 2016, **359**, 110–123.
59 C. R. Doran and A. Aschengrau, Prenatal and early childhood exposure to tetrachloroethylene (PCE)-contaminated drinking water and sleep quality in adulthood, *Environ. Health*, 2022, **21**, 15.
60 A. Yu Alentiev, E. Drioli, M. Gokzhaev, G. Golemme, O. Ilinich, A. Lapkin, V. Volkov and Y. Yampolskii, Gas permeation properties of phenylene oxide polymers, *J. Membr. Sci.*, 1998, **138**, 99–107.
61 G. Chowdhury, R. Vujosevic, T. Matsuura and B. Laverty, Effects of polymer molecular weight and chemical modification on the gas transport properties of poly(2,6-dimethyl-1,4-phenylene oxide), *J. Appl. Polym. Sci.*, 2000, **77**, 1137–1143.
62 Y.-J. Fu, C.-L. Lai, J.-T. Chen, C.-T. Liu, S.-H. Huang, W.-S. Hung, C.-C. Hu and K.-R. Lee, Hydrophobic composite membranes for separating of water-alcohol mixture by pervaporation at high temperature, *Chem. Eng. Sci.*, 2014, **111**, 203–210.
63 M. Soniat, M. Tesfaye, A. Mafi, D. J. Brooks, N. D. Humphrey, L.-C. Weng, B. Merinov, W. A. Goddard, A. Z. Weber and F. A. Houle, Permeation of CO_2 and N_2 through glassy poly(dimethyl phenylene) oxide under steady- and presteady-state conditions, *J. Polym. Sci.*, 2020, **58**, 1207–1228.
64 Y. Wu, Z. Guo, H. Wu, K. Zhu, L. Yang, L. Ren, Y. Liu, X. Wu, R. Zhao, N. AliKhan, N. M. Ahmad, M. Younas and Z. Jiang, Plasticization- and aging-resistant membranes with venation-like architecture for efficient carbon capture, *J. Membr. Sci.*, 2020, **609**, 118215.